

# Origin of the Springtime Westerly Bias in Equatorial Atlantic Surface Winds in the Community Atmosphere Model Version 3 (CAM3) Simulation

CHING-YEE CHANG, SUMANT NIGAM, AND JAMES A. CARTON

*Department of Atmospheric and Oceanic Science, University of Maryland, College Park, College Park, Maryland*

(Manuscript received 6 July 2007, in final form 24 January 2008)

## ABSTRACT

This study makes the case that westerly bias in the surface winds of the National Center for Atmospheric Research (NCAR) Community Atmosphere Model, version 3 (CAM3), over the equatorial Atlantic in boreal spring has its origin in the rainfall (diabatic heating) bias over the tropical South American continent. The case is made by examination of the spatiotemporal evolution of regional precipitation and wind biases and by dynamical diagnoses of the westerly wind bias from experiments with a steady, linearized dynamical core of an atmospheric general circulation model. Diagnostic modeling indicates that underestimating rainfall over the eastern Amazon region can lead to the westerly bias in equatorial Atlantic surface winds.

The study suggests that efforts to reduce coupled model biases, especially seasonal ones, must target continental biases, even in the deep tropics where ocean–atmosphere interaction generally rules.

## 1. Introduction

Trade winds (easterlies) prevail over most of the tropical Atlantic and Pacific Oceans through the course of the year and are strongest in the northern tropics in boreal winter. Their seasonal fluctuation has a profound influence on sea surface temperature in the central and eastern basins, and vice versa. Along the equator, easterly winds generate equatorial upwelling and cold SST, but not simultaneously across all longitudes: cold SSTs first appear in the far eastern basin. Their leading edge then moves westward, generating a tongue of cold SST, which is maximally extended in August–September. The easterlies relax in boreal spring in conjunction with the deepening of the thermocline and appearance of warm SSTs in the eastern basin.

Simulation of the seasonal cycle of the equatorial trade winds is, however, challenging for both atmospheric and coupled ocean–atmosphere–land general circulation models (AGCM/CGCM) (Davey et al. 2002; Okumura and Xie 2004; DeWitt 2005; Chang et al. 2007). Davey et al. showed the equatorial zonal wind stress to be too weak in many nonflux-corrected

CGCMs. Okumura and Xie (2004) found equatorial westerlies to prevail over the eastern half of the basin in winter and spring in an AGCM. DeWitt (2005) showed the weak zonal wind stress along the equator to be the likely cause of the simulated zonal SST-gradient error. The westerly bias in the Atlantic trade winds is, thus, a common simulation deficiency, but one whose origin remains unclear.

The present study seeks to investigate the cause of the westerly wind bias, especially along the equator, in the National Center for Atmospheric Research's (NCAR) Community Atmosphere Model, version 3 (CAM3; Collins et al. 2006a), and the Community Climate System Model, version 3 (CCSM3; Collins et al. 2006b), simulations. The wind bias in these simulations was documented in Chang et al. (2007), who also examined the bias in related atmospheric and oceanic fields. These authors noted with interest the accompaniment of surface westerly bias by upper-level (200 hPa) easterly bias and deficient (excess) rainfall over the Amazon (Africa) in the simulations, that is, a weaker Walker circulation in the Atlantic sector. The westerly bias in surface winds was also linked to the anomalously deep CCSM3 thermocline. Based on bias structures, Chang et al. discuss potential causes of the bias, suggesting deficient rainfall over the Amazon as one possibility.

Local mechanisms have also been proposed to ac-

---

*Corresponding author address:* Sumant Nigam, 3419 Computer and Space Sciences Bldg., University of Maryland, College Park, College Park, MD 20742.  
E-mail: nigam@atmos.umd.edu

count for the westerly trade wind bias in model simulations. These include insufficient generation of stratus clouds (Yu and Mechoso 1999) and coastal upwelling (Large and Danabasoglu 2006), but whether they are the symptoms or the cause remains to be seen. The notion that deficient Amazonian rainfall can be the ultimate cause of Atlantic sector biases in atmospheric and oceanic fields is an interesting, but heretical one as two decades of ENSO research has emphasized the primacy of ocean–atmosphere coupling in shaping variability in/over the tropical oceans. Land–atmosphere coupling has, however, been shown to be important in initiating and setting the pace of seasonal variability over the tropical oceans, the eastern basins in particular, through the timing and location (e.g., coastline orientation) of continental convection (e.g., Mitchell and Wallace 1992). The Atlantic basin is, if anything, more susceptible to land influences than the eastern tropical Pacific because of its smaller zonal extent, sandwiched between two major continental convection centers (Amazonia to the west and Africa to the east).

The present study investigates the hypothesis that deficient Amazonian rainfall is the root cause of the westerly bias in equatorial surface winds over the Atlantic. While the hypothesis can be fully tested only with an AGCM experiment, a diagnostic modeling analysis is presented to make the case. The magnitude and extent of the influence of Amazonian latent heating deficiencies on surface winds is computed using a steady, linearized dynamical core of an AGCM. The diagnostic model is described in section 2 along with the datasets used in this study. The seasonal evolution of westerly wind, precipitation, and diabatic heating biases and related evidence that prompted the hypothesis on the controlling influence of Amazonian convection is presented in section 3. Dynamical diagnosis of the CAM3 westerly bias in equatorial Atlantic surface winds, including those establishing the viability of the model, is presented in section 4. Synopsis and concluding remarks follow in section 5 in which westerly wind and rainfall biases from a recent CAM development simulation are presented in support of the case made in this study.<sup>1</sup>

## 2. Datasets and diagnostic model

### a. Simulation datasets

The model simulations analyzed here are the same as in Chang et al. (2007). The mean of a five-member

<sup>1</sup> The simulation was generated with a CAM development model (CAM3\_3\_fv\_cmt2\_dilute) that incorporated improvements to the deep convection scheme (Richter–Neale).

ensemble of T-85 resolution CAM3 Atmospheric Model Intercomparison Project (AMIP) simulations is analyzed.<sup>2</sup> The CCSM3 simulations come from the 20th Century Climate in Coupled Models project of the Intergovernmental Panel on Climate Change and are archived as case b30.030a (20C3M run1) on the Program for Climate Model Diagnosis and Intercomparison (PCMDI) Web site. This coupled integration, initiated in 1870, is forced by historical ozone, solar, volcanic, greenhouse gases, and sulfur dioxide/trioxide distributions.

### b. Precipitation

Monthly precipitation analysis, based on satellite and gauge measurements, comes from the Global Precipitation Climatology Project (GPCP) version 2 (Adler et al. 2003). Data is available on a  $2.5^\circ \times 2.5^\circ$  grid over both land and ocean for the 1979–2006 period.

### c. ERA-40 atmospheric analysis

The ECMWF global 40-yr reanalysis (ERA-40) (Upala et al. 2005) spans September 1957–August 2002 and is locally available on a  $2.5^\circ$  global grid and 23 levels in the vertical. The reanalysis combines model forecast fields, satellite data, radiosonde, and other in situ data, including aircraft and ship reports, with three-dimensional variational (3DVAR) data assimilation. The ERA-40 assimilation model is the modified ECMWF Integrated Forecasting System, which is a T-159 spectral resolution model with 60 vertical levels. The 1979–onward reanalysis, benefiting from inclusion of satellite data, is used in assessing model simulations and in generating the basic state and forcing fields for the diagnostic model.

### d. Surface winds

Surface wind speed estimates (combined with wind directions from ECMWF analysis) are available on a  $1^\circ \times 1^\circ$  longitude–latitude grid for the 1988–2000 period from the Special Sensor Microwave Imager (SSM/I) (Atlas et al. 1996), and this record is supplemented by the Quick Scatterometer (QuikSCAT) winds (Graf et al. 1998) for the period from mid-1999 to 2006.

### e. Diagnosed diabatic heating

Diabatic heating was diagnosed in-house using the ERA-40 isobaric reanalyses at  $2.5^\circ$  resolution (Chan

<sup>2</sup> These simulations are referred to as the “vanilla-AMIP” since they have no external forcing beyond the supplied SST field, as opposed to the “IPCC-AMIP” runs in which volcano, greenhouse gases, aerosols, and solar-related external forcing are additionally applied.

and Nigam 2008). Heating was diagnosed as a residual in the thermodynamic equation (e.g., Hoskins et al. 1989; Nigam 1994) using monthly-averaged data and submonthly transient fluxes, as it was earlier for the National Centers for Environmental Protection (NCEP) and ERA-15 reanalyses in Nigam et al. (2000).

#### f. Diagnostic model

The steady linear primitive equation (SLPE) model solves the  $\sigma$ -coordinate ( $=p/p_s$ , where  $p_s$  is surface pressure) primitive equations. The equations are linearized about a zonally symmetric basic state, and the model solves for the eddy component (i.e., deviation from the zonal average) of the circulation. The linearized model equations are given in the appendix of Held et al. (1989). To realistically represent the thermal and momentum diffusion processes in the planetary boundary layer, the simplified Rayleigh momentum dissipation and Newtonian temperature damping terms in these equations are replaced by linearized versions of the vertical momentum and thermal diffusion terms (Nigam 1997). The diffusion coefficients vary in the boundary layer, decreasing rapidly above 925 hPa. The inclusion of diffusive mixing leads to lower boundary conditions on zonal and meridional velocity and temperature, requiring specification of drag coefficients  $C_{DU}$ ,  $C_{DV}$ , and  $C_{DT}$ . In addition to vertical diffusive mixing in the planetary boundary layer, the thermodynamic and horizontal momentum equations include horizontal diffusive mixing with a constant coefficient of  $1 \times 10^6 \text{ m}^2 \text{ s}^{-1}$ . Additional model details can be found in the appendix of Nigam (1994) and Nigam and Chung (2000). All model parameters are specified exactly as in Nigam (1997), except for the drag coefficients  $C_{DU}$  and  $C_{DV}$ , which are both set equal to  $1.0 \times 10^{-3}$  instead of  $1.5 \times 10^{-3}$ .

The diagnostic model is solved numerically using the semispectral representation for horizontal structure: 73 grid points between the two poles ( $\Delta\theta = 2.5^\circ$ ) and zonal Fourier truncation at wavenumber 30 (equivalent to  $\Delta\lambda = 6.0^\circ$ ), where  $\theta$  is latitude and  $\lambda$  longitude. The vertical structure is discretized using 18 full-sigma levels, of which 14 are in the troposphere, including 5 below 850 hPa. The semispectral model was preferred in view of strong latitudinal variation of tropical features, such as the intertropical convergence zone.

### 3. CAM3 biases in the tropical Atlantic

#### a. Westerly wind bias

The seasonal evolution of surface zonal wind at the equator is shown in the upper panels of Fig. 1 at

monthly resolution.<sup>3</sup> Both satellite-based wind observations and ERA-40 reanalysis capture the seasonal cycle—annual in the western basin and semiannual in the eastern basin—quite well. Model simulations fare well in the latter half of the calendar year, but not in boreal spring when westerlies are present in most basin longitudes and not just the eastern sector (as in observations). The westerly bias in modeled surface winds is extensively documented in Chang et al. (2007), who show the entire deep tropics ( $10^\circ\text{S}$ – $10^\circ\text{N}$ ) to be biased, with the zonal-wind bias peaking at the equator; see their Fig. 4. The westerly bias is evidently amplified in the presence of an interactive ocean as the CCSM3 bias is twice as large, and a bit delayed as well. The westerly bias effectively changes the character of seasonal variability in the eastern basin from semiannual to annual, especially in the CCSM3 simulation.

An intercomparison of observed and modeled zonal wind evolution (Fig. 1, upper panels), especially the slope of westerly wind contours in the winter-to-spring months, initially suggested an eastern origin of the bias, tempering efforts to connect the bias (and the weaker Walker circulation) with Amazonian rainfall. Plotting the bias itself, however, clarifies the situation: the CAM3 bias with respect to ERA-40 (Fig. 1, lower middle panel) shows the westerlies to originate in the western sector, for example, from tracking of the  $+2 \text{ m s}^{-1}$  contour. Not all of the surface zonal-wind bias in the Atlantic basin originates in the western sector though. The slope of the  $+1 \text{ m s}^{-1}$  contour indicates the presence of a westward propagating bias as well. This bias component is, however, not the dominant one in winter and early spring when the largest bias is developing.

#### b. Precipitation bias

The precipitation bias structure provides further insight into the origin of the westerly bias. The CAM3 bias in Amazonian and African precipitation with respect to GPCP rainfall is shown in Fig. 1, lower left and right panels, with the panel lineup according to regional geography. Immediately apparent is the big deficit in eastern Amazon rainfall ( $6$ – $7 \text{ mm day}^{-1}$ ) and its timing. The maximum deficit is in March, that is, during the peak of the local rainy season. Interestingly, the deficit develops near synchronously with the westerly bias, which peaks in March–April. The wind bias lags Amazon rainfall by, at most, a month. The CAM3 bias relative to ERA-40 rainfall (not shown) is very similar. The

<sup>3</sup> The 20-yr simulation climatologies are only marginally different from the 50-yr climatologies shown in Chang et al. (2007).

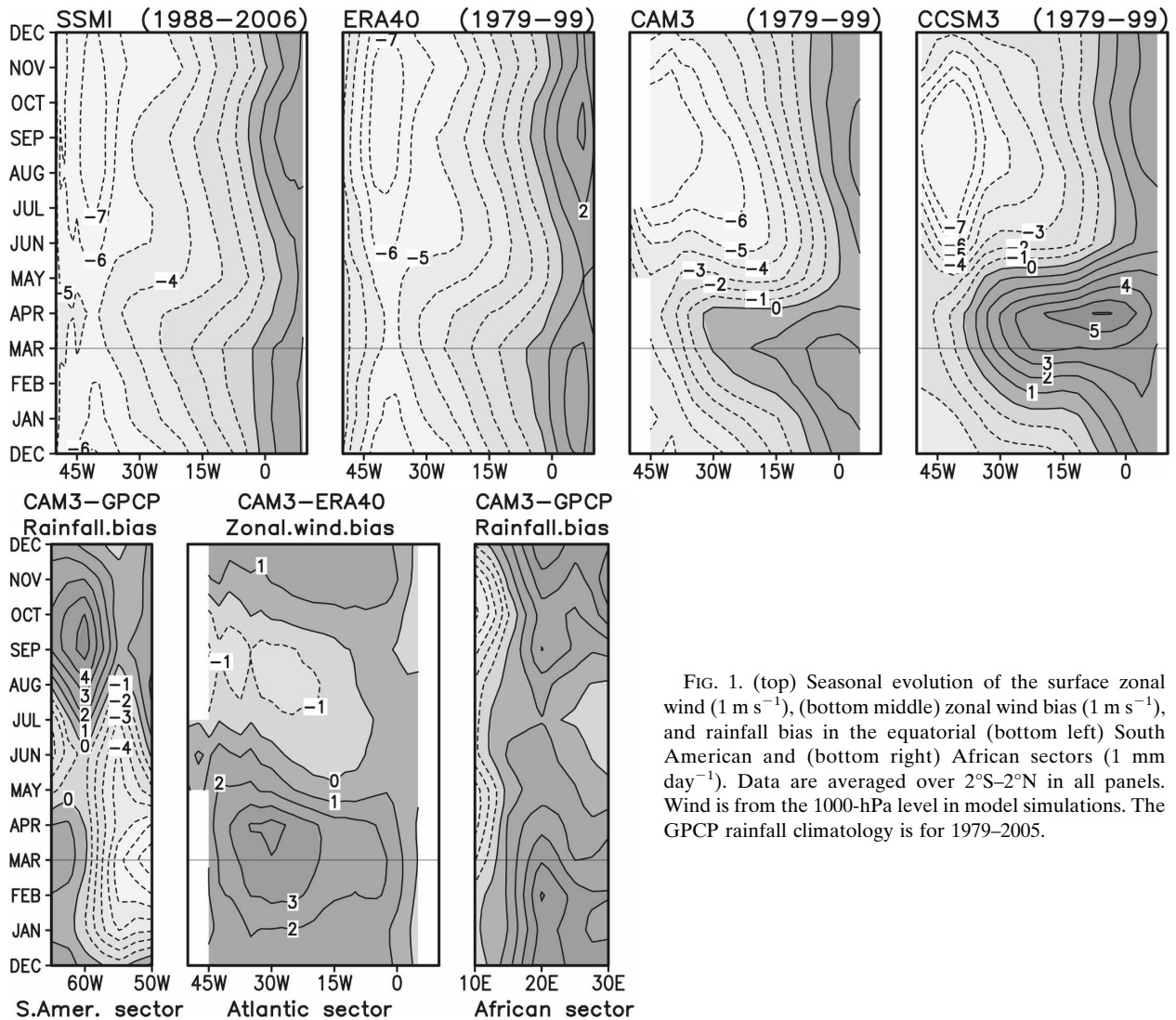


FIG. 1. (top) Seasonal evolution of the surface zonal wind ( $1 \text{ m s}^{-1}$ ), (bottom middle) zonal wind bias ( $1 \text{ m s}^{-1}$ ), and rainfall bias in the equatorial (bottom left) South American and (bottom right) African sectors ( $1 \text{ mm day}^{-1}$ ). Data are averaged over  $2^{\circ}\text{S}$ – $2^{\circ}\text{N}$  in all panels. Wind is from the 1000-hPa level in model simulations. The GPCP rainfall climatology is for 1979–2005.

spatiotemporal structure of the eastern Amazon rainfall deficit and the downstream westerly wind bias thus provide strong, albeit circumstantial, evidence for an Amazonian origin of the Atlantic Walker circulation bias in CAM3/CCSM3 simulations.

The connection of the westerly bias with simulation errors in African rainfall—the other anchor point of the Atlantic Walker circulation—is examined in the lower right panel of Fig. 1. Unlike over the Amazon, CAM3 generates excessive rainfall over much of Africa. The year-round excess is typically  $3\text{--}4 \text{ mm day}^{-1}$  except in summer when it is lower. Evolution of the westerly bias in the eastern basin indicates some susceptibility to the African rainfall errors. Diagnostic modeling analysis (discussed later), however, shows the Amazon influence to dominate over most of the Atlantic basin.

The off-equatorial distribution of observed and simu-

lated precipitation over the Amazon and surrounding regions (land and ocean) is displayed in Fig. 2 (left panels) for the peak westerly bias period, March–May. The CAM3 bias shows rainfall over tropical South America to be deficient, especially over the eastern Amazon ( $-5 \text{ mm day}^{-1}$ ) and Andes ( $-2 \text{ mm day}^{-1}$ ); in both cases, the deficiency is as large as  $\sim 50\%$  of the local climatology and thus quite significant. The rainfall deficits are reflected in the diabatic heating distribution, which is shown next.

### c. Diabatic heating bias

Diabatic heating, generated from both cloud-scale and large-scale processes, is the principal forcing of the tropical circulation. The latent heating component is dominant in the deep tropics, especially in regions of

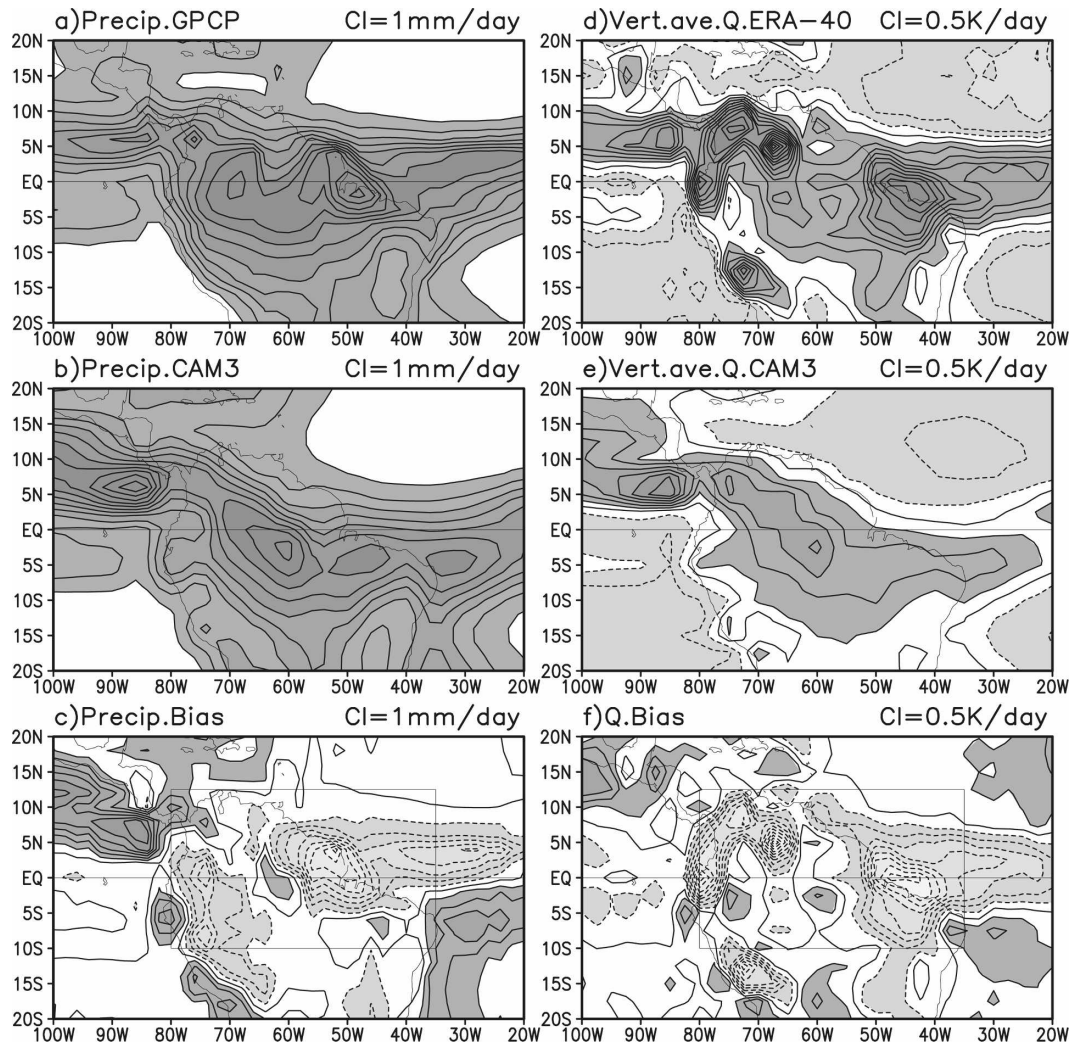


FIG. 2. Climatological March–May (left) precipitation ( $1 \text{ mm day}^{-1}$ ) and (right) diabatic heating ( $0.5 \text{ K day}^{-1}$ ) distribution over tropical South America in observations and CAM3 simulation with (top) observationally derived fields, (middle) CAM3, and the (bottom) CAM3 bias (e.g., CAM3 – ERA-40). ERA-40 heating is from a residual diagnosis. The surface-to-125-hPa vertical average (mass weighted) in the 1979–2002 period climatology is shown. The marked rectangle in the bottom panels indicates the tropical region whose influence is subsequently investigated.

deep convection, such as the intertropical convergence zone, the western Pacific warm pool, and the Amazon. A close correspondence between precipitation and vertically averaged diabatic heating is expected in these regions, and this expectation is borne out in Fig. 2 (right panels). The correspondence is particularly striking in the middle panels, in which both fields are from CAM3. Note the similar location of the field maxima. The correspondence in the top panels is not as striking since the fields are from different sources and because residual diagnosis of heating in regions of steep orography is more uncertain, especially if the underlying circulation and temperature analyses are not well anchored by ob-

servations—the case over most of South America. Even so, the correspondence over the eastern Amazon is notable and is manifest in the similarity of this region's heating and precipitation biases.

#### 4. Dynamical diagnosis of the CAM3 westerly bias in surface winds

Modeling analysis that provides insight into the origin of the CAM3 westerly bias over the equatorial Atlantic is reported here. The dynamical diagnosis is conducted using a diagnostic model, a choice that needs some justification in view of vigorous ocean–atmo-

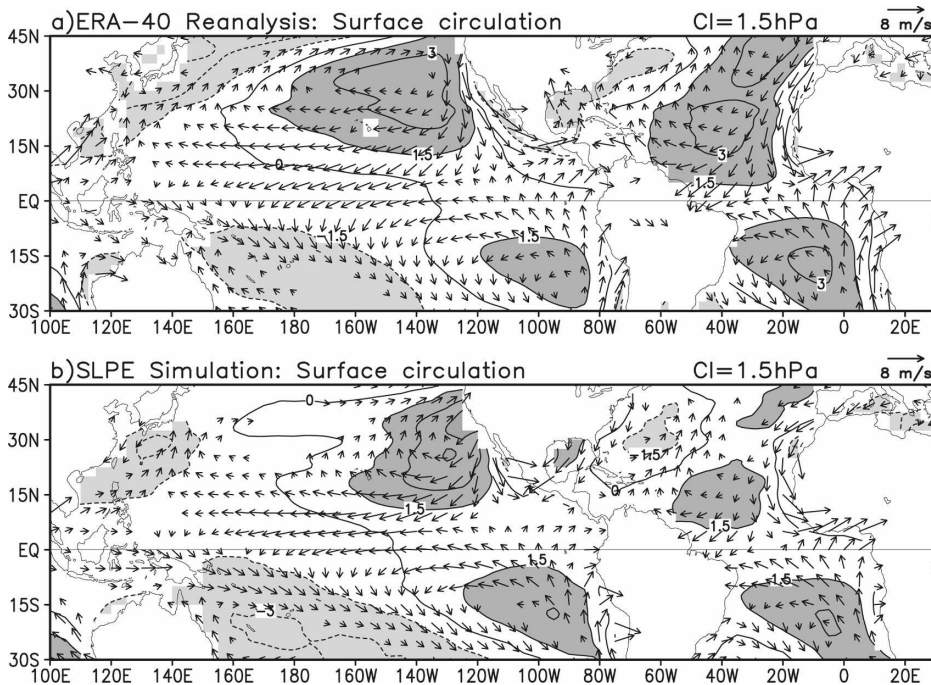


FIG. 3. Observed (ERA-40) and diagnostically simulated March–May surface circulation (zonally asymmetric part) in the Pacific and Atlantic sectors: (a) Sea level pressure and 1000-hPa winds from ERA-40 and (b) their simulation from the SLPE model, using the same contour interval and vector scale. The SLPE model is forced by orography, 3D diabatic heating, and submonthly thermal and vorticity transient fluxes, all obtained/diagnosed from ERA-40. Wind vectors are not plotted when the wind speed is less than  $1 \text{ m s}^{-1}$ . Values over land are masked out prior to computation of the zonally asymmetric component.

sphere–land interaction in the tropics. As noted before, the westerly bias is present in both CAM3 and CCSM3 simulations, albeit more robustly in the latter, indicating that this bias is not rooted in ocean–atmosphere interactions. The same, however, cannot be said for land–atmosphere interactions since rainfall generation and distribution is governed by a number of processes including those dependent on the land surface state. The use of an atmosphere-only diagnostic model, as here, therefore, can be limiting, especially if the analysis goal extends beyond identification of the geographic regions exerting unrealistic local and remote influences. The present analysis seeks only such identification in context of the CAM3 Atlantic biases, deferring further analysis of the causes of aberrant model behavior over the South American continent to a later study.

A prerequisite for dynamical diagnosis is the diagnostic model's ability to simulate the target field: the CAM3 Atlantic bias. If notable features of the bias can be simulated, its origin can be investigated, at least in a diagnostic (a posteriori) sense. For a meaningful analysis, the model should be required to simulate the indi-

vidual circulations (observed, CAM3) as well.<sup>4</sup> This assessment is made in Fig. 3, which shows the observed and diagnostically simulated March–May surface circulations after removal of the zonal-mean component; that is, only the eddy components are shown. The zonal-mean component is removed as the diagnostic model is linearized about it, making this circulation component common to the target and simulated fields.

#### a. Model assessment: March–May simulation

In the Fig. 3 simulation, the zonal-mean zonal and meridional velocities, temperature, and surface pressure from ERA-40 are the 2D model inputs (basic state specification), and orography, surface temperature, and diagnosed 3D diabatic heating and submonthly transient heat and momentum fluxes are the model forcing. The surface circulation, consisting of sea level pressure (SLP) and 1000-hPa winds, is of direct interest in view

<sup>4</sup> Or better yet, their average: The bias ( $a - b$ ) and average ( $a + b$ ) are independent states, and a model that simulates both offers prospects for a more insightful analysis.

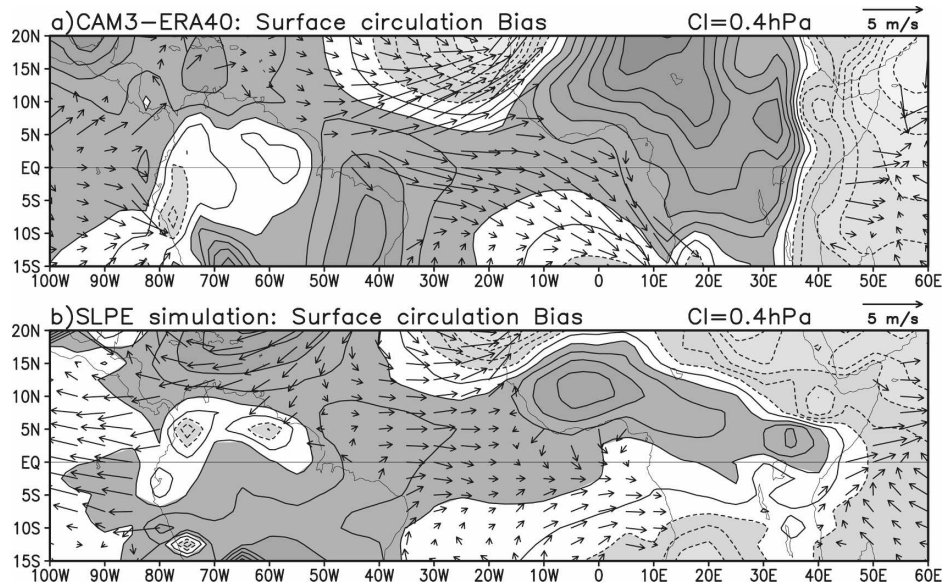


FIG. 4. The CAM3 (a) surface circulation bias and (b) diagnostic simulation with the zonally asymmetric part of sea level pressure and 1000-hPa winds shown as in Fig. 3. The diagnostic simulation is obtained without thermal and mechanical transient forcing bias. The SLP contour interval and wind vector scale are indicated in the title line; positive (negative) SLP bias exceeding 0.4 hPa is shaded dark (light).

of the westerly surface wind bias: both observed (ERA-40) and simulated surface fields are shown. The SLP high in the tropical and subtropical Atlantic (and Pacific) is reasonably simulated except for the amplitude; the midlatitude simulation is even better. In the tropics, where SLP is no longer a proxy for the winds, the simulated trade winds are weak in the northern, but not southern, tropical Atlantic. The reasonable simulation of ERA-40's March–May surface circulation clears the way for the next level of model assessment: its potential in simulating the CAM3 bias.

#### b. Model assessment: Bias simulation

The simulated CAM3 bias is shown in Fig. 4 with the target fields in the top panel. The simulation is obtained without transient forcing, mechanical or thermal, and as the difference of two diagnostic model solutions: one obtained with ERA-40 zonal-mean basic state, surface temperature, orography, and diagnosed 3D diabatic heating; the other with the CAM3 counterparts. The thermal and mechanical transient forcing is not applied in each case, in part because the submonthly transient fluxes were unavailable in the CAM3 archive. Note that the zonally varying component of the SLP and 1000-hPa winds are displayed in both cases.

The bias simulation is reasonable, but not as remarkable as the simulation of the ERA-40 surface circulation (cf. Fig. 3), in part because of the missing impact of

transient fluxes, which can be significant, especially outside of the deep tropics. The CAM3 westerly bias in the equatorial Atlantic is, nonetheless, captured albeit with weaker amplitude, just as in Fig. 3. The westerly bias cannot all be attributed to heating differences in view of other model-input differences (orography, surface temperature, and zonal-mean basic state). The latter differences are eliminated in the following section through the use of ERA-40 fields in both cases.

#### c. Diagnosis of the CAM3 equatorial westerly bias

The geographic region whose heating contributes most to the westerly bias in the equatorial Atlantic is identified in this section from diagnostic modeling. The circulation bias is modeled as the difference between two linear simulations that differ only in the specification of diabatic heating in selected regions. The common specification of all other model inputs in the two simulations (from ERA-40), including zonal-mean basic state, allows unambiguous attribution of the CAM3 westerly bias to regional heating biases. Such a differencing strategy also filters out the diagnostic model's own simulation bias (cf. Fig. 3).

The surface circulation forced by the global tropical (15°S–15°N) heating bias is shown in Fig. 5a. Almost all of the SLP bias ( $\sim 1$  hPa) and westerly wind bias ( $\sim 3$  m s $^{-1}$ ) in the western equatorial Atlantic originates, not surprisingly, in the tropics. Note the smaller (half) SLP

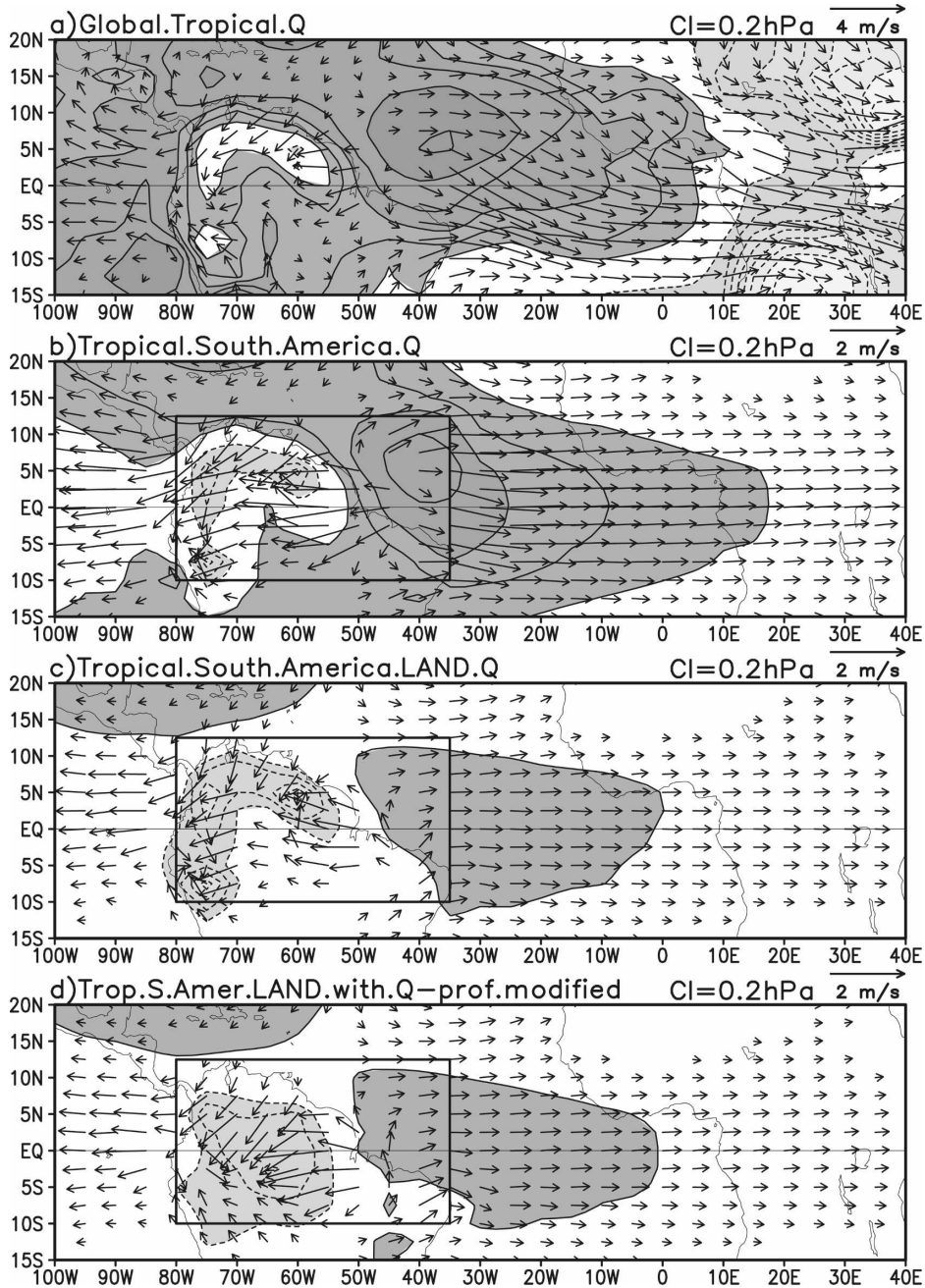


FIG. 5. Diagnostic analysis of the CAM3 March–May surface circulation bias: (a) global tropical (15°S–15°N) heating bias, (b) tropical South American (marked box) heating bias, (c) tropical South American continental heating bias, and (d) synthetic continental heating bias. The latter is obtained by multiplying vertically averaged heating by the average heating profile over the tropical South American land mass. SLP contour interval (half as in Fig. 4) and wind vector scale are indicated in the title line; vector scale in top panel is twice as large as in others; bias vectors of less than 0.2 m s<sup>-1</sup> wind speed are not plotted; positive (negative) SLP bias exceeding 0.2 hPa is shaded dark (light).

contour interval in Fig. 5. Only the surface simulation is displayed owing to limited space. The influence of regional heating biases in the tropics is examined next, beginning with the South American (10°S–

12.5°N, 80°–35°W; marked rectangle in Fig. 5b). Comparison indicates that between half and two-thirds of the westerly bias attributed to the tropics (Fig. 5a) originates in the South American region. The sector's influ-

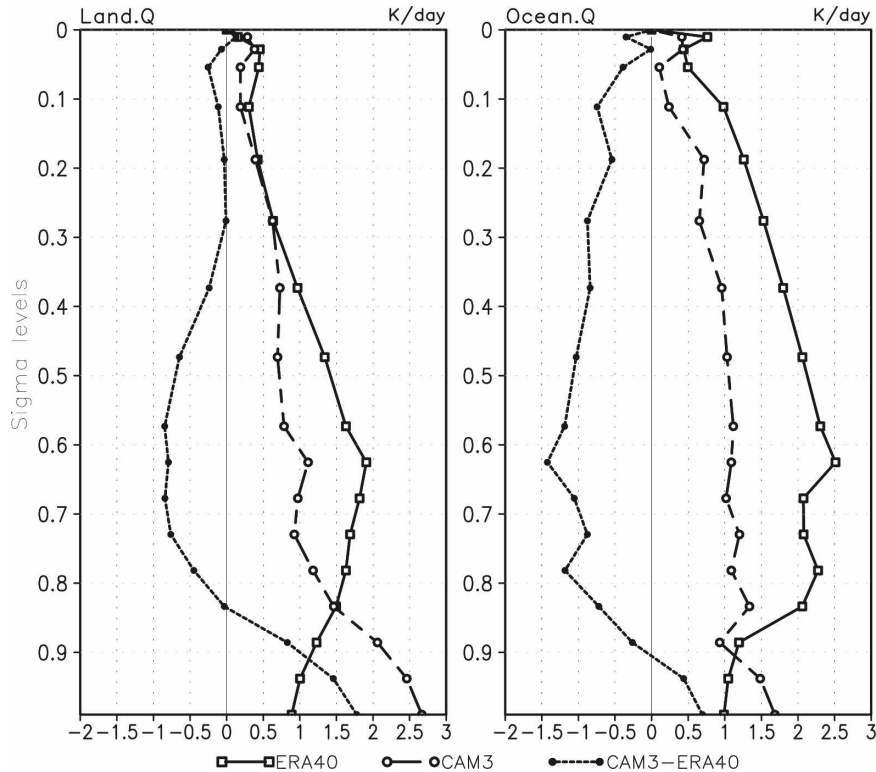


FIG. 6. Diabatic heating profiles over the tropical South American region: average profile over the (left) continental and (right) oceanic regions of the box marked in Fig. 5. Both observationally constrained (ERA-40 residual diagnosis) and CAM3-simulated profiles are shown along with the CAM3 bias.

ence is far from local, extending up to the African shores. The maximum westerly response,  $\sim 1.6 \text{ m s}^{-1}$ , is located  $\sim 30^\circ\text{W}$ , that is, close to the location of the CAM3 peak westerly bias. Structure of the surface response, with westerlies to the east of the eastern Amazon cooling (cf. Fig. 3) and easterlies to its west, indicates weaker surface convergence and ascending motion over the eastern Amazon in CAM3.

The next two panels parse the Fig. 5b response into parts forced by the heating bias over land and ocean sectors. The surface circulation forced by the continental heating bias is shown in Fig. 5c. Its structure is similar to the total response (Fig. 5b) but the amplitude is smaller, being one-third to half of the latter. The continent forced westerly bias is  $\sim 0.6 \text{ m s}^{-1}$  at  $30^\circ\text{W}$ : This is significant, especially since continental convection biases are less labile than oceanic ones in part because the land surface state (e.g., soil moisture) cannot change as readily as SST can from equatorial and coastal upwelling. Efforts to reduce coupled model biases, especially seasonal ones, must target the biases in continental regions. A large body of work on seasonal cycle variability in the eastern tropical Pacific [beginning with Mitchell and Wallace's

(1992) study, and including Xie (1996) and Nigam and Chao (1996), among others] would also argue for this strategy.

The CAM3 simulation differs from ERA-40, not only in the horizontal distribution of vertically averaged diabatic heating (and, thus, precipitation in the tropics), but also in its vertical structure. The heating profiles for the South American region are shown in Fig. 6, separately for the land and ocean sectors.<sup>5</sup> The CAM3 profile is quite distinct from the ERA-40 profile, particularly over land where it is weaker (stronger) in the mid (lower) troposphere. The excessive low-level heating in CAM3 results from strong sensible heating arising from warmer than observed land surface temperature (not shown). The CAM3 difference from ERA-40, also plotted, is, interestingly, a mirror image of the heating pro-

<sup>5</sup> The profiles are displayed using the  $\sigma (p/p_s)$  vertical coordinate to preclude intercomparison of fictitious below-ground pressure-level heating data, given significant orography in the region. This vertical coordinate, however, portrays the regional midtropospheric ( $\sim 500 \text{ hPa}$ ) heating maximum as a lower-tropospheric feature owing to lower surface pressure ( $p_s$ ) over elevated regions.

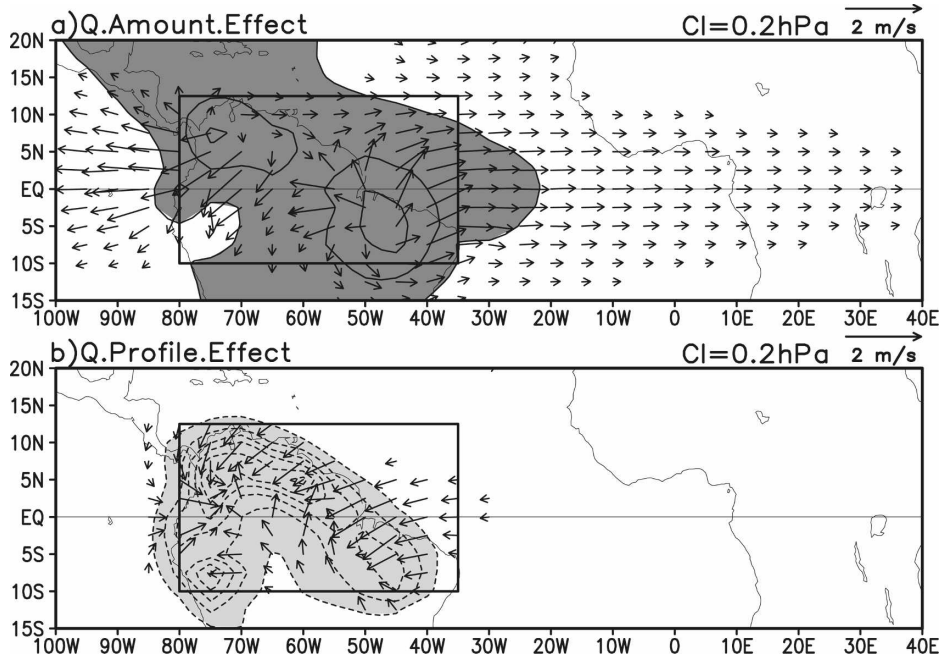


FIG. 7. Diagnostic analysis of the CAM3 March–May surface circulation bias: bias forced by synthetic heating over the tropical South American continent (land in the marked box), consisting of only the (a) CAM3 heating *amount* bias, and (b) CAM3 heating *profile* bias.

file typically associated with stratiform convection (cf. Houze 1997), potentially, reflecting undersimulation of stratiform rainfall in CAM3.

The heating profile is very influential in the deep tropics since latent heating is largely offset by ascent-induced adiabatic cooling there, resulting in the pressure vertical velocity ( $\omega$ ) mimicking the heating profile ( $N^2\omega \approx Q$ , where  $N^2$  is static stability and  $Q$  the diabatic heating rate). The heating vertical structure is thus directly tied to the divergent circulation through the continuity equation and to the rotational flow via the stretching term of the vorticity equation. Thus, it is of some interest to examine if the heating amount or heating profile differences are more consequential in the context of the CAM3 westerly bias.

The influence of heating profile differences is assessed by computing the model's response to synthetic heating distributions. These are obtained from multiplication of the vertically averaged heating field by the regionally averaged heating profile, resulting in each grid point of the region having the same heating vertical structure. The synthetic distributions are assessed in Fig. 5d, which shows the model response forced by the heating bias over tropical South America, as in Fig. 5c, except for the use of synthetic CAM3 and ERA-40 heating. The close similarity of surface circulations in Figs. 5c and 5d attests to the viability of this analysis

strategy in ascertaining the role of profile differences in generation of the CAM3 westerly wind bias over the equatorial Atlantic.

The influence of the South American land heating bias is shown in Fig. 7 with the amount and profile effects separated out. In the top panel, the CAM3 heating was modified to have the same profile as ERA-40 heating while still retaining the amount of bias. The resulting surface response shows that the westerly bias attributed to the heating bias over tropical South America (cf. Figs. 5c and 5d) arises largely from the heating amount rather than profile differences. The impact of the profile bias on surface circulation (Fig. 7b) was found to be significant as well, but confined to the continental forcing region. The heating profile bias over tropical South America evidently contributes little to the Atlantic westerly bias.

It is interesting to note the opposite sign of the South American SLP response generated by the amount and profile biases in Fig. 7. The positive SLP in the former case arises from reduced latent heating amount (in midtroposphere) with concomitant reduction in offsetting ascent and, thus, low-level convergence, all consistent with a positive SLP response. The negative SLP response in the profile case arises from excessive low-level heating (and midtroposphere cooling) in CAM3 (cf. left panel in Fig. 6), whose compensation requires

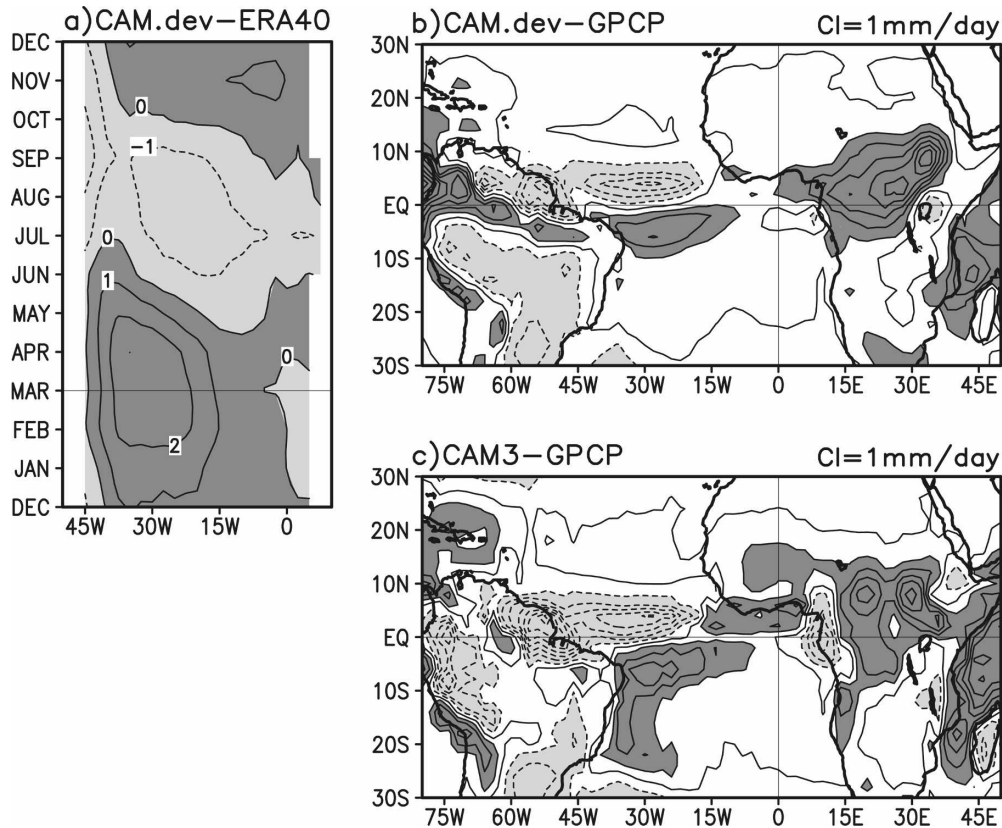


FIG. 8. (left) Surface zonal wind and (right) tropical precipitation biases in a CAM3 development simulation (Richter–Neale deep convection; see footnote 1 for more details). The CAM3 precipitation bias in an expanded tropical sector is also shown to facilitate comparison.

ascent and low-level convergence in the near-surface levels, thus, a negative SLP signal.<sup>6</sup>

## 5. Concluding remarks

This study makes the case that westerly bias in the CAM3 surface winds over the equatorial Atlantic in boreal spring, and indeed, also in the corresponding coupled model's (CCSM3) surface winds, has its origin in the rainfall (diabatic heating) bias over the tropical South American continent. The case is made from examination of the spatiotemporal evolution of regional precipitation and wind biases and from dynamical diagnoses of the westerly wind bias from experiments with a steady, linearized dynamical core of an atmospheric general circulation model. Diagnostic modeling

indicates that underestimation of rainfall over the eastern Amazon region can lead to westerly bias in equatorial Atlantic surface winds.

A continental origin for a key coupled model bias in the deep tropics seems somewhat far-fetched at first in view of vigorous ocean–atmosphere interaction in equatorial regions, for example, during El Niño–Southern Oscillation variability. Implicating deficient modeling of land–atmosphere interaction (leading to diminished continental convection and rainfall) as the source of the downstream westerly bias, however, seems more reasonable upon further reflection, especially in view of the large body of work on seasonal variability in the eastern tropical Pacific, beginning with Mitchell and Wallace (1992). Their analysis showed continental convection to be the “pacemaker” in seasonal climate evolution in the eastern tropical basins. (Seasonal variability in these regions is pronouncedly annual despite incident insolation being dominantly semiannual.)

Important support for the South American origin of the Atlantic westerly wind bias comes from a recent

<sup>6</sup> By the same token, sinking and horizontally divergent flow must occur in the midtroposphere, with higher pressure there. From a column perspective, opposite-signed circulations occur at different levels, but these mass-balanced flows provide limited insight into the hydrostatic basis for the resulting SLP response.

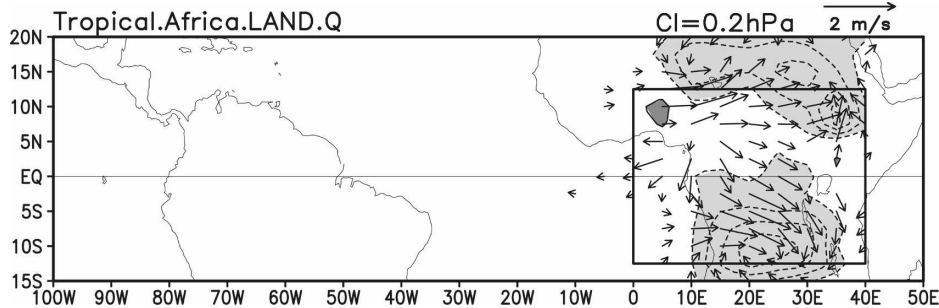


FIG. 9. Diagnostic analysis of the CAM3 March–May surface circulation bias: response of the tropical African continental (marked box) heating bias.

CAM development simulation (see fn 1 for more details). The simulation was produced at NCAR in early 2007 using a CAM3 version that included improvements to the deep convection scheme. The westerly bias in the equatorial Atlantic and rainfall bias in the tropical American–Atlantic–African sector are displayed in Fig. 8. Immediately apparent is the significant reduction in the westerly wind bias by more than  $1 \text{ m s}^{-1}$  (cf. Fig. 1). Also notably diminished is the rainfall bias over the eastern Amazon (and Andean region) but not the ITCZ/rainfall bias over the tropical Atlantic, which is only marginally weaker. The new bias structures support the claim for a defining role of eastern Amazon rainfall deficiencies in generation of the westerly bias in equatorial Atlantic surface winds.

Our analysis would be incomplete without addressing the role of the African rainfall bias in generating a westerly bias over the equatorial Atlantic. The African bias is broadly of the opposite sign, and is about half as large as the eastern Amazon bias, especially in the CAM development simulation; biases of both signs are present along the coast in CAM3. If the African bias were influential, a larger westerly wind bias should be in evidence in the development simulation in view of the coherent and stronger positive rainfall bias in this case. The westerly bias is, however, notably diminished in this simulation (cf. Fig. 8). Diagnostic modeling also indicates the influence of the African rainfall (diabatic heating) bias to be largely confined to the far eastern basin (Fig. 9), supporting the assessment of a limited role of the African rainfall bias in generation of the westerly bias in the western/central equatorial Atlantic basin.

Finally, it is of some interest to inquire about the fate of the westerly bias in a coupled ocean–atmosphere environment. The bias is larger in CCSM3 (cf. Fig. 1), as noted before, indicating the lack of any corrective/negative feedbacks in this coupled model. Chang et al. (2007) argue that the westerly bias leads to a deeper thermocline (and warmer SSTs) in the eastern equato-

rial basin with the SST-gradient change generating additional westerlies (cf. Lindzen and Nigam 1987), that is, for the existence of a positive feedback that amplifies the bias.

**Acknowledgments.** The authors thank Steven C. Chan for providing access to the diabatic heating field diagnosed from ERA-40 in advance of the publication of the related paper, Alfredo Ruiz-Barradas and Renu R. Joseph for their help in acquiring the CAM3 and CCSM3 datasets, and Semyon A. Grodsky and Jin-Ho Yoon for their helpful discussions. Sumant Nigam wishes to acknowledge the support of Grants NOAA/CPPA NA17EC1483 and NSF ATM-0649666.

#### REFERENCES

- Adler, R. F., and Coauthors, 2003: The Version-2 Global Precipitation Climatology Project (GPCP) monthly precipitation analysis (1979–present). *J. Hydrometeorol.*, **4**, 1147–1167.
- Atlas, R., R. Hoffman, S. Bloom, J. Jusem, and J. Ardizzone, 1996: A multiyear global surface wind velocity data set using SSM/I wind observations. *Bull. Amer. Meteor. Soc.*, **77**, 869–882.
- Chan, S., and S. Nigam, 2008: Residual diagnosis of diabatic heating from ERA-40 and NCEP reanalyses: Intercomparisons with TRMM. *J. Climate*, in press.
- Chang, C.-Y., J. A. Carton, S. A. Grodsky, and S. Nigam, 2007: Seasonal climate of the tropical Atlantic sector in the NCAR Community Climate System Model 3: Error structure and probable causes of errors. *J. Climate*, **20**, 1053–1070.
- Collins, W. D., and Coauthors, 2006a: The Community Climate System Model version 3 (CCSM3). *J. Climate*, **19**, 2122–2143.
- , and Coauthors, 2006b: The formulation and atmospheric simulation of the Community Atmosphere Model version 3 (CAM3). *J. Climate*, **19**, 2144–2161.
- Davey, M., and Coauthors, 2002: STOIC: A study of coupled model climatology and variability in tropical ocean regions. *Climate Dyn.*, **18**, 403–420.
- DeWitt, D. G., 2005: Diagnosis of the tropical Atlantic near-equatorial SST bias in a directly coupled atmosphere–ocean general circulation model. *Geophys. Res. Lett.*, **32**, L01703, doi:10.1029/2004GL021707.
- Graf, J., C. Sasaki, C. Winn, W. T. Liu, W. Tsai, M. Freilich, and

- D. Long, 1998: NASA Scatterometer Experiment. *Acta Astronaut.*, **43**, 397–407.
- Held, I. M., S. W. Lyons, and S. Nigam, 1989: Transients and the extratropical response to El Niño. *J. Atmos. Sci.*, **46**, 163–174.
- Hoskins, B. J., H. H. Hsu, I. N. James, M. Masutani, P. D. Sardeshmukh, and G. H. White, 1989: Diagnostics of the global atmospheric circulation based on ECMWF analyses 1979–1989. WCRP-27, WMO Tech. Doc. 326, 217 pp.
- Houze, R. A., Jr., 1997: Stratiform precipitation in regions of convection: A meteorological paradox? *Bull. Amer. Meteor. Soc.*, **78**, 2179–2196.
- Large, W. G., and G. Danabasoglu, 2006: Attribution and impacts of upper-ocean biases in CCSM3. *J. Climate*, **19**, 2325–2346.
- Lindzen, R. S., and S. Nigam, 1987: On the role of sea surface temperature gradients in forcing low-level winds and convergence in the tropics. *J. Atmos. Sci.*, **44**, 2418–2436.
- Mitchell, T. P., and J. M. Wallace, 1992: The annual cycle in equatorial convection and sea surface temperature. *J. Climate*, **5**, 1140–1156.
- Nigam, S., 1994: On the dynamical basis for the Asian summer monsoon rainfall–El Niño relationship. *J. Climate*, **7**, 1750–1771.
- , 1997: The annual warm to cold phase transition in the eastern equatorial Pacific: Diagnosis of the role of stratus cloud-top cooling. *J. Climate*, **10**, 2447–2467.
- , and Y. Chao, 1996: Evolution dynamics of tropical ocean–atmosphere annual cycle variability. *J. Climate*, **9**, 3187–3205.
- , and C. Chung, 2000: ENSO surface winds in CCM3 simulation: Diagnosis of errors. *J. Climate*, **13**, 3172–3186.
- , —, and E. DeWeaver, 2000: ENSO diabatic heating in ECMWF and NCEP–NCAR reanalyses, and NCAR CCM3 simulation. *J. Climate*, **13**, 3152–3171.
- Okumura, Y., and S.-P. Xie, 2004: Interaction of the Atlantic equatorial cold tongue and the African monsoon. *J. Climate*, **17**, 3589–3602.
- Uppala, S. M., and Coauthors, 2005: The ERA-40 Re-Analysis. *Quart. J. Roy. Meteor. Soc.*, **131**, 2961–3012.
- Xie, S. P., 1996: Westward propagation of latitudinal asymmetry in a coupled ocean–atmosphere model. *J. Atmos. Sci.*, **53**, 3236–3250.
- Yu, J.-Y., and C. R. Mechoso, 1999: A discussion on the errors in the surface heat fluxes simulated by a coupled GCM. *J. Climate*, **12**, 416–426.